Benchmarking 6DOF Outdoor Visual Localization in Changing Conditions

Torsten Sattler[1] Will Maddern[2] Carl Toft[3] Akihiko Torii[4] Lars Hammarstrand[3]
Erik Stenborg[3] Daniel Safari[4,5] Masatoshi Okutomi[4] Marc Pollefeys[1,6]
Josef Sivic[7,8] Fredrik Kahl[3,9] Tomas Pajdla[8]
[1]Department of Computer Science, ETH Zürich [2]Oxford Robotics Institute, University of Oxford
[3]Department of Electrical Engineering, Chalmers University of Technology [6]Microsoft
[4]Tokyo Institute of Technology [5]Technical University of Denmark [7]Inria*
[8]CIIRC, CTU in Prague† [9]Centre for Mathematical Sciences, Lund University

Abstract

Visual localization enables autonomous vehicles to navigate in their surroundings and augmented reality applications to link virtual to real worlds. Practical visual localization approaches need to be robust to a wide variety of viewing condition, including day-night changes, as well as weather and seasonal variations, while providing highly accurate 6 degree-of-freedom (6DOF) camera pose estimates. In this paper, we introduce the first benchmark datasets specifically designed for analyzing the impact of such factors on visual localization. Using carefully created ground truth poses for query images taken under a wide variety of conditions, we evaluate the impact of various factors on 6DOF camera pose estimation accuracy through extensive experiments with state-of-the-art localization approaches. Based on our results, we draw conclusions about the difficulty of different conditions, showing that long-term localization is far from solved, and propose promising avenues for future work, including sequence-based localization approaches and the need for better local features. Our benchmark is available at `visuallocalization.net`.

1. Introduction

Estimating the 6DOF camera pose of an image with respect to a 3D scene model is key for visual navigation of autonomous vehicles and augmented/mixed reality devices. Solutions to this *visual localization* problem can also be used to "close loops" in the context of SLAM or to register images to Structure-from-Motion (SfM) reconstructions.

Work on 3D structure-based visual localization has focused on increasing efficiency [30, 33, 39, 52, 66], improving scalability and robustness to ambiguous structures [32, 50, 65, 73], reducing memory requirements [12, 33, 50], and more flexible scene representations [54]. All these methods utilize local features to establish 2D-3D matches. These correspondences are in turn used to estimate the camera pose. This data association stage is critical as pose estimation fails without sufficiently many correct matches. There is a well-known trade-off between discriminative power and invariance for local descriptors. Thus, existing localization approaches will only find enough matches if both the query images and the images used to construct the 3D scene model are taken under similar viewing conditions.

Figure 1. Visual localization in changing urban conditions. We present three new datasets, *Aachen Day-Night*, *RobotCar Seasons* (shown) and *CMU Seasons* for evaluating 6DOF localization against a prior 3D map (top) using registered query images taken from a wide variety of conditions (bottom), including day-night variation, weather, and seasonal changes over long periods of time.

Capturing a scene under all viewing conditions is prohibitive. Thus, the assumption that all relevant conditions are covered is too restrictive in practice. It is more realistic to expect that images of a scene are taken under a single or a few conditions. To be practically relevant, *e.g.*, for

*WILLOW project, Departement d'Informatique de l'École Normale Supérieure, ENS/INRIA/CNRS UMR 8548, PSL Research University.

†CIIRC - Czech Institute of Informatics, Robotics, and Cybernetics, Czech Technical University in Prague

life-long localization for self-driving cars, visual localization algorithms need to be robust under varying conditions (*cf*. Fig. 1). Yet, no work in the literature actually measures the impact of varying conditions on 6DOF pose accuracy.

One reason for the lack of work on visual localization under varying conditions is a lack of suitable benchmark datasets. The standard approach for obtaining ground truth 6DOF poses for query images is to use SfM. An SfM model containing both the database and query images is built and the resulting poses of the query images are used as ground truth [33, 54, 61]. Yet, this approach again relies on local feature matches and can only succeed if the query and database images are sufficiently similar [49]. The benchmark datasets constructed this way thus tend to only include images that are relatively easy to localize in the first place.

In this paper, we construct the first datasets for benchmarking visual localization under changing conditions. To overcome the above mentioned problem, we heavily rely on human work: We manually annotate matches between images captured under different conditions and verify the resulting ground truth poses. We create three complimentary benchmark datasets based on existing data [4, 41, 55]. All consist of a 3D model constructed under one condition and offer query images taken under different conditions: The *Aachen Day-Night* dataset focuses on localizing high-quality night-time images against a day-time 3D model. The *RobotCar Seasons* and *CMU Seasons* dataset both consider automotive scenarios and depict the same scene under varying seasonal and weather conditions. One challenge of the RobotCar Seasons dataset is to localize low-quality night-time images. The CMU Seasons dataset focuses on the impact of seasons on vegetation and thus the impact of scene geometry changes on localization.

This paper makes the following **contributions**: *(i)* We create a new outdoor benchmark complete with ground truth and metrics for evaluating 6DOF visual localization under changing conditions such as illumination (day/night), weather (sunny/rain/snow), and seasons (summer/winter). Our benchmark covers multiple scenarios, such as pedestrian and vehicle localization, and localization from single and multiple images as well as sequences. *(ii)* We provide an extensive experimental evaluation of state-of-the-art algorithms from both the computer vision and robotics communities on our datasets. We show that existing algorithms, including SfM, have severe problems dealing with both day-night changes and seasonal changes in vegetated environments. *(iii)* We show the value of querying with multiple images, rather than with individual photos, especially under challenging conditions. *(iv)* We make our benchmarks publicly available at `visuallocalization.net` to stimulate research on long-term visual localization.

2. Related Work

Localization benchmarks. Tab. 1 compares our benchmark datasets with existing datasets for both visual localization and place recognition. Datasets for place recognition [15, 43, 63, 67, 69] often provide query images captured under different conditions compared to the database images. However, they neither provide 3D models nor 6DOF ground truth poses. Thus, they cannot be used to analyze the impact of changing conditions on pose estimation accuracy. In contrast, datasets for visual localization [14, 26, 28, 32, 33, 54, 55, 58, 61] often provide ground truth poses. However, they do not exhibit strong changes between query and database images due to relying on feature matching for ground truth generation. A notable exception is the Michigan North Campus Long-Term (NCLT) dataset [13], providing images captured over long period of time and ground truth obtained via GPS and LIDAR-based SLAM. Yet, it does not cover all viewing conditions captured in our datasets, *e.g.*, it does not contain any images taken at night or during rain. To the best of our knowledge, ours are the first datasets providing both a wide range of changing conditions and accurate 6DOF ground truth. Thus, ours is the first benchmark that measures the impact of changing conditions on pose estimation accuracy.

Datasets such as KITTI [23], TorontoCity [71], or the Málaga Urban dataset [6] also provide street-level image sequences. Yet, they are less suitable for visual localization as only few places are visited multiple times.

3D structure-based localization methods [32, 33, 36, 50, 52, 65, 73] establish correspondences between 2D features in a query image and 3D points in a SfM point cloud via descriptor matching. These 2D-3D matches are then used to estimate the query's camera pose. Descriptor matching can be accelerated by prioritization [16, 33, 52] and efficient search algorithms [19, 39]. In large or complex scenes, descriptor matches become ambiguous due to locally similar structures found in different parts of the scene [32]. This results in high outlier ratios of up to 99%, which can be handled by exploiting co-visibility information [32, 36, 50] or via geometric outlier filtering [9, 65, 73].

We evaluate *Active Search* [52] and the *City-Scale Localization* approach [65], a deterministic geometric outlier filter based on a known gravity direction, as representatives for efficient respectively scalable localization methods.

2D image-based localization methods approximate the pose of a query image using the pose of the most similar photo retrieved from an image database. They are often used for place recognition [1, 15, 38, 51, 64, 67] and loop-closure detection [18, 22, 45]. They remain effective at scale [3, 51, 54, 69] and can be robust to changing conditions [1, 15, 46, 54, 64, 67]. We evaluate two compact VLAD-based [27] image-level representations: DenseVLAD [67]

Dataset	Setting	Image Capture	3D SfM Model (# Sub-Models)	# Images		Condition Changes			6DOF query poses
				Database	Query	Weather	Seasons	Day-Night	
Alderley Day/Night [43]	Suburban	Trajectory		14,607	16,960	✓		✓	
Nordland [63]	Outdoors	Trajectory		143k			✓		
Pittsburgh [68]	Urban	Trajectory		254k	24k				
SPED [15]	Outdoors	Static Webcams		1.27M	120k	✓	✓	✓	
Tokyo 24/7 [67]	Urban	Free Viewpoint		75,984	315			✓	
7 Scenes [58]	Indoor	Free Viewpoint		26,000	17,000				✓
Aachen [55]	Historic City	Free Viewpoint	1.54M / 7.28M (1)	3,047	369				
Cambridge [28]	Historic City	Free Viewpoint	1.89M / 17.68M (5)	6,848	4,081				✓(SfM)
Dubrovnik [33]	Historic City	Free Viewpoint	1.89M / 9.61M (1)	6,044	800				✓(SfM)
Landmarks [32]	Landmarks	Free Viewpoint	38.19M / 177.82M (1k)	204,626	10,000				
Mall [61]	Indoor	Free Viewpoint		682	2296				✓
NCLT [13]	Outdoors & Indoors	Trajectory		about 3.8M			✓		✓
Rome [33]	Landmarks	Free Viewpoint	4.07M / 21.52M (69)	15,179	1000				
San Francisco [14, 32, 54]	Urban	Free Viewpoint	30M / 149M (1)	610,773	442				✓(SfM)
Vienna [26]	Landmarks	Free Viewpoint	1.12M / 4.85M (3)	1,324	266				
Aachen Day-Night (ours)	Historic City	Free Viewpoint	1.65M / 10.55M (1)	4,328	922			✓	✓
RobotCar Seasons (ours)	Urban	Trajectory	6.77M / 36.15M (49)	20,862	11,934	✓	✓	✓	✓
CMU Seasons (ours)	Suburban	Trajectory	1.61M / 6.50M (17)	7,159	75,335	✓	✓		✓

Table 1. Comparison with existing benchmarks for place recognition and visual localization. "Condition Changes" indicates that the viewing conditions of the query images and database images differ. For some datasets, images were captured from similar camera trajectories. If SfM 3D models are available, we report the number of sparse 3D points and the number of associated features. Only our datasets provide a diverse set of changing conditions, reference 3D models, and most importantly ground truth 6DOF poses for the query images.

aggregates densely extracted SIFT descriptors [2, 37] while NetVLAD [1] uses learned features. Both are robust against day-night changes [1, 67] and work well at large-scale [54].

We also evaluate the de-facto standard approach for loop-closure detection in robotics [20, 34], where robustness to changing conditions is critical for long-term autonomous navigation [15, 35, 43, 46, 64, 67]: FAB-MAP [18] is an image retrieval approach based on the Bag-of-Words (BoW) paradigm [60] that explicitly models the co-occurrence probability of different visual words.

Sequence-based approaches for image retrieval are used for loop-closure detection in robotics [40, 43, 47]. Requiring a matched sequence of images in the correct order significantly reduces false positive rates compared to single-image retrieval approaches, producing impressive results including direct day-night matches with SeqSLAM [43]. We evaluate OpenSeqSLAM [63] on our benchmark.

Multiple cameras with known relative poses can be modelled as a generalized camera [48], *i.e.*, a camera with multiple centers of projections. Approaches for absolute pose estimation for both multi-camera systems [31] and camera trajectories [10] from 2D-3D matches exist. Yet, they have never been applied for localization in changing conditions. In this paper, we show that using multiple images can significantly improve performance in challenging scenarios.

Learning-based localization methods have been proposed to solve both loop-closure detection [15, 42, 62, 64] and pose estimation [17, 28, 57, 70]. They learn features with stable appearance over time [15, 44, 46], train classifiers for place recognition [11, 24, 35, 72], and train CNNs to regress 2D-3D matches [7, 8, 58] or camera poses [17, 28, 70].

3. Benchmark Datasets for 6DOF Localization

This section describes the creation of our three new benchmark datasets. Each dataset is constructed from publicly available data, allowing our benchmarks to cover multiple geographic locations. We add ground truth poses for all query images and build reference 3D models (*cf*. Fig. 3) from images captured under a single condition.

All three datasets present different challenges. The *Aachen Day-Night* dataset focuses on localizing night-time photos against a 3D model built from day-time imagery. The night-time images, taken with a mobile phone using software HDR post-processing, are of high quality. The dataset represents a scenario where images are taken with hand-held cameras, *e.g.*, an augmented reality application.

Both the *RobotCar Seasons* and the *CMU Seasons* datasets represent automotive scenarios, with images captured from a car. In contrast to the Aachen Day dataset, both datasets exhibit less variability in viewpoints but a larger variance in viewing conditions. The night-time images from the RobotCar dataset were taken from a driving car with a consumer camera with auto-exposure. This results in significantly less well-lit images exhibiting motion blur, *i.e.*, images that are significantly harder to localize (*cf*. Fig. 2).

The RobotCar dataset depicts a mostly urban scene with rather static scene geometry. In contrast, the CMU dataset contains a significant amount of vegetation. The changing appearance and geometry of the vegetation, due to seasonal changes, is the main challenge of this dataset.

3.1. The Aachen Day-Night Dataset

Our Aachen Day-Night dataset is based on the Aachen localization dataset from [55]. The original dataset contains 4,479 reference and 369 query images taken in the old inner city of Aachen, Germany. It provides a 3D SfM model but does not have ground truth poses for the queries. We augmented the original dataset with day- and night-time queries captured using standard consumer phone cameras.

To obtain ground truth poses for the day-time queries, we used COLMAP [56] to create an intermediate 3D model

	reference model				query images
	# images	# 3D points	# features	condition	conditions (# images)
Aachen Day-Night	4,328	1.65M	10.55M	day	day (824), night (98)
RobotCar Seasons	20,862	6.77M	36.15M	overcast (November)	dawn (1,449), dusk (1,182), night (1,314), night+rain (1,320), rain (1,263), overcast summer / winter (1,389 / 1,170), snow (1,467), sun (1,380)
CMU Seasons	7,159	1.61M	6.50M	sun / no foliage (April)	sun (22,073), low sun (28,045), overcast (11,383), clouds (14,481), foliage (33,897), mixed foliage (27,637), no foliage (13,801) urban (31,250), suburban (13,736), park (30,349)

Table 2. Detailed statistics for the three benchmark datasets proposed in this paper. For each dataset, a reference 3D model was constructed using images taken under the same reference condition, *e.g.*, "overcast" for the RobotCar Seasons dataset.

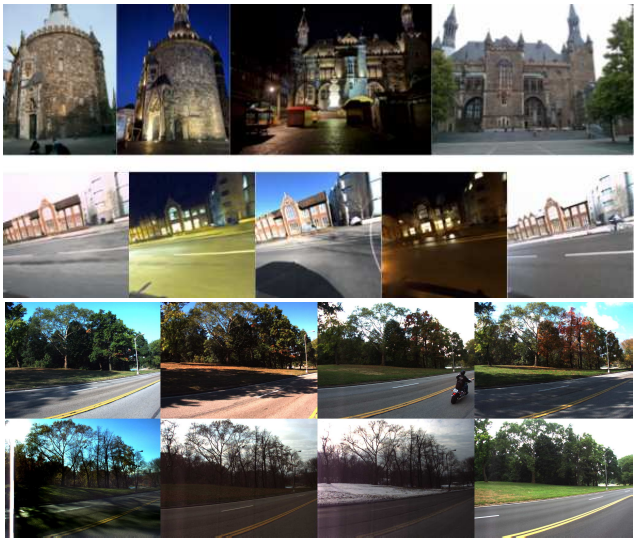

Figure 2. Example query images for *Aachen Day-Night* (top), *RobotCar Seasons* (middle) and *CMU Seasons* datasets (bottom).

from the reference and day-time query images. The scale of the reconstruction is recovered by aligning it with the geo-registered original Aachen model. As in [33], we obtain the reference model for the Aachen Day-Night dataset by removing the day-time query images. 3D points visible in only a single remaining camera were removed as well [33]. The resulting 3D model has 4,328 reference images and 1.65M 3D points triangulated from 10.55M features.

Ground truth for night-time queries. We captured 98 night-time query images using a Google Nexus5X phone with software HDR enabled. Attempts to include them in the intermediate model resulted in highly inaccurate camera poses due to a lack of sufficient feature matches. To obtain ground truth poses for the night-time queries, we thus hand-labelled 2D-3D matches. We manually selected a day-time query image taken from a similar viewpoint for each night-time query. For each selected day-time query, we projected its visible 3D points from the intermediate model into it. Given these projections as reference, we manually labelled 10 to 30 corresponding pixel positions in the night-time query. Using the resulting 2D-3D matches and the known intrinsics of the camera, we estimate the camera poses using a 3-point solver [21, 29] and non-linear pose refinement.

To estimate the accuracy for these poses, we measure the mean reprojection error of our hand-labelled 2D-3D correspondences (4.33 pixels for 1600x1200 pixel images) and the pose uncertainty. For the latter, we compute multiple poses from a subset of the matches for each image and measure the difference in these poses to our ground truth poses. The mean median position and orientation errors are 36cm and 1°. The absolute pose accuracy that can be achieved by minimizing a reprojection error depends on the distance of the camera to the scene. Given that the images were typically taken 15 or more meters from the scene, we consider the ground truth poses to be reasonably accurate.

3.2. The RobotCar Seasons Dataset

Our RobotCar Seasons dataset is based on a subset of the publicly available Oxford RobotCar Dataset [41]. The original dataset contains over 20M images recorded from an autonomous vehicle platform over 12 months in Oxford, UK. Out of the 100 available traversals of the 10km route, we select one reference traversal in overcast conditions and nine query traversals that cover a wide range of conditions (*cf*. Tab. 2). All selected images were taken with the three synchronized global shutter Point Grey Grasshopper2 cameras mounted to the left, rear, and right of the car. Both the intrinsics of the cameras and their relative poses are known.

The reference traversal contains 26,121 images taken at 8,707 positions, with 1m between successive positions. Building a single consistent 3D model from this data is very challenging, both due to sheer size and the lack of visual overlap between the three cameras. We thus built 49 non-overlapping local submaps, each covering a 100m trajectory. For each submap, we initialized the database camera poses using vehicle positions reported by the inertial navigation system (INS) mounted on the RobotCar. We then iteratively triangulated 3D points, merged tracks, and refined both structure and poses using bundle adjustment. The scale of the reconstructions was recovered by registering them against the INS poses. The reference model contains all submaps and consists of 20,862 reference images and 6.77M 3D points triangulated from 36.15M features.

We obtained query images by selecting reference positions inside the 49 submaps and gathering all images from the nine query traversals with INS poses within 10m of one of the positions. This resulted in 11,934 images in total, where triplets of images were captured at 3,978 distinct locations. We also grouped the queries into 460 temporal sequences based on the timestamps of the images.

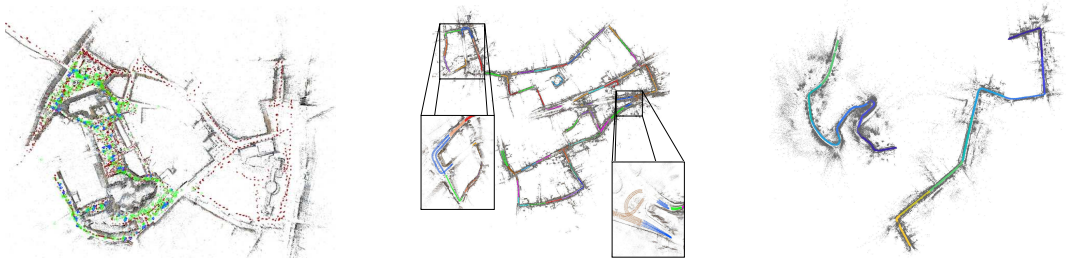

Figure 3. 3D models of the *Aachen Day-Night* (left, showing database (red), day-time query (green), and night-time query images (blue)), *RobotCar Seasons* (middle), and *CMU Seasons* (right) datasets. For RobotCar and CMU, the colors encode the individual submaps.

Ground truth poses for the queries. Due to GPS drift, the INS poses cannot be directly used as ground truth. Again, there are not enough feature matches between day- and night-time images for SfM. We thus used the LIDAR scanners mounted to the vehicle to build local 3D point clouds for each of the 49 submaps under each condition. These models were then aligned to the LIDAR point clouds of the reference trajectory using ICP [5]. Many alignments needed to be manually adjusted to account for changes in scene structure over time (often due to building construction and road layout changes). The final median RMS errors between aligned point clouds was under 0.10m in translation and 0.5° in rotation across all locations. The alignments provided ground truth poses for the query images.

3.3. The CMU Seasons Dataset

The CMU Seasons Dataset is based on a subset of the CMU Visual Localization Dataset [4], which contains more than 100K images recorded by the Computer Vision Group at Carnegie Mellon University over a period of 12 months in Pittsburgh, PA, USA. The images were collected using a rig of two cameras mounted at 45 degree forward/left and forward/right angles on the roof of an SUV. The vehicle traversed an 8.5 km long route through central and suburban Pittsburgh 16 times with a spacing in time of between 2 weeks up to 2 months. Out of the 16 traversals, we selected the one from April 4 as the reference, and then 11 query traversals were selected such that they cover the range of variations in seasons and weather that the data set contains.

Ground truth poses for the queries. As with the RobotCar dataset, the GPS is not accurate enough and the CMU dataset is also too large to build one 3D model from all the images. The full sequences were split up into 17 shorter sequences, each containing about 250 consecutive vehicle poses. For each short sequence, a 3D model was built using bundle adjustment of SIFT points tracked over several image frames. The resulting submaps of the reference route were merged with the corresponding submaps from the other traversals by using global bundle adjustment and manually annotated image correspondences. Reprojection errors are within a few pixels for all 3D points and the distances between estimated camera positions and expected ones (based on neighbouring cameras) are under 0.10m. The resulting reference model consists of 1.61M 3D points triangulated from 6.50M features in 7,159 database images. We provide 75,335 query images and 187 query sequences.

4. Benchmark Setup

We evaluate state-of-the-art localization approaches on our new benchmark datasets to measure the impact of changing conditions on camera pose estimation accuracy and to understand how hard robust long-term localization is.

Evaluation measures. We measure the *pose accuracy* of a method by the deviation between the estimated and the ground truth pose. The *position error* is measured as the Euclidean distance $\|c_{\text{est}} - c_{\text{gt}}\|_2$ between the estimated c_{est} and the ground truth position c_{gt}. The absolute *orientation error* $|\alpha|$, measured as an angle in degrees, is computed from the estimated and ground truth camera rotation matrices $\mathtt{R}_{\text{est}}$ and $\mathtt{R}_{\text{gt}}$. We follow standard practice [25] and compute $|\alpha|$ as $2\cos(|\alpha|) = \text{trace}(\mathtt{R}_{\text{gt}}^{-1}\mathtt{R}_{\text{est}}) - 1$, *i.e.*, we measure the minimum rotation angle required to align both rotations [25].

We measure the percentage of query images localized within Xm and $Y°$ of their ground truth pose. We define three pose accuracy intervals by varying the thresholds: *High-precision* (0.25m, 2°), *medium-precision* (0.5m, 5°), and *coarse-precision* (5m, 10°). These thresholds were chosen to reflect the high accuracy required for autonomous driving. We use the intervals (0.5m, 2°), (1m, 5°), (5m, 10°) for the Aachen night-time queries to account for the higher uncertainty in our ground truth poses. Still, all regimes are more accurate than consumer-grade GPS systems.

Evaluated algorithms. As discussed in Sec. 2, we evaluate a set of state-of-the-art algorithms covering the most common types of localization approaches: From the class of 3D structure-based methods, we use *Active Search* (AS) [54] and *City-Scale Localization* (CSL) [65]. From the class of 2D image retrieval-based approaches, we use *DenseVLAD* [67], *NetVLAD* [1], and *FAB-MAP* [18].

In order to measure the benefit of using multiple images for pose estimation, we evaluate two approaches: *OpenSeqSLAM* [63] is based on image retrieval and enforces that the images in the sequence are matched in correct order. Knowing the relative poses between the query images, we can model them as a generalized camera [48]. Given 2D-3D

matches per individual image (estimated via Active Search), we estimate the pose via a generalized absolute camera pose solver [31] inside a RANSAC loop. We denote this approach as *Active Search+GC* (AS+GC). We mostly use ground truth query poses to compute the relative poses that define the generalized cameras[1]. Thus, AS+GC provides an upper bound on the number of images that can be localized when querying with generalized cameras.

The methods discussed above all perform localization from scratch without any prior knowledge about the pose of the query. In order to measure how hard our datasets are, we also implemented two *optimistic baselines*. Both assume that a set of relevant database images is known for each query. Both perform pairwise image matching and use the known ground truth poses for the reference images to triangulate the scene structure. The feature matches between the query and reference images and the known intrinsic calibration are then be used to estimate the query pose. The first optimistic baseline, *LocalSfM*, uses upright RootSIFT features [2, 37]. The second uses upright CNN features densely extracted on a regular grid. We use the same VGG-16 network [59] as NetVLAD. The *DenseSfM* method uses coarse-to-fine matching with conv4 and conv3 features.

We select the relevant reference images for the two baselines as follows: For Aachen, we use the manually selected day-time image (*cf*. Sec. 3.1) to select up to 20 reference images sharing the most 3D points with the selected day-time photo. For RobotCar and CMU, we use all reference images within 5m and 135° of the ground truth query pose.

We evaluated *PoseNet* [28] but were not able to obtain competitive results. We also attempted to train *DSAC* [7] on KITTI but were not able to train it. Both PoseNet and DSAC were thus excluded from further evaluations.

5. Experimental Evaluation

This section presents the second main contribution of this paper, a detailed experimental evaluation on the effect of changing conditions on the pose estimation accuracy of visual localization techniques. In the following, we focus on pose accuracy. Please see [53] for experiments concerning computation time.

5.1. Evaluation on the Aachen Day-Night Dataset

The focus of the Aachen Day-Night dataset is on benchmarking the pose accuracy obtained by state-of-the-art methods when localizing night-time queries against a 3D model constructed from day-time imagery. In order to put the results obtained for the night-time queries into context, we first evaluate a subset of the methods on the 824 day-time queries. As shown in Tab. 3, the two structure-based methods are able to estimate accurate camera poses and localize nearly all images within the coarse-precision regime. We conclude that the Aachen dataset is not particularly challenging for the day-time query images.

[1]Note that Active Search+GC only uses the relative poses between the query images to define the geometry of a generalized camera. It does *not* use any information about the absolute poses of the query images.

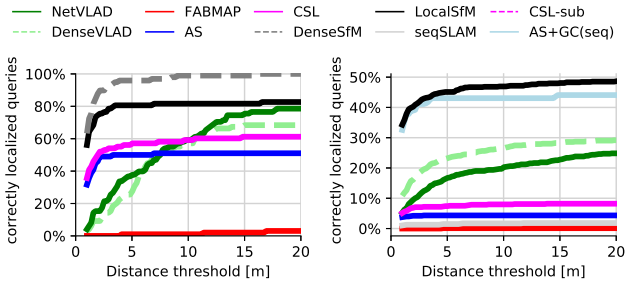

Figure 4. Cumulative distribution of position errors for the night-time queries of the Aachen (left) and RobotCar (right) datasets.

Night-time queries. Tab. 3 also reports the results obtained for the night-time queries. We observe a significant drop in pose accuracy for both Active Search and CSL, down from above 50% in the high-precision regime to less than 50% in the coarse-precision regime. Given that the night-time queries were taken from similar viewpoints as the day-time queries, this drop is solely caused by the day-night change.

CSL localizes more images compared to Active Search (AS). This is not surprising since CSL also uses matches that were rejected by AS as too ambiguous. Still, there is a significant difference to LocalSfM. CSL and AS both match features against the full 3D model while LocalSfM only considers a small part of the model for each query. This shows that global matching sufficiently often fails to find the correct nearest neighbors, likely caused by significant differences between day-time and night-time descriptors.

Fig. 4(left) shows the cumulative distribution of position errors for the night-time queries and provides interesting insights: LocalSfM, despite knowing relevant reference images for each query, completely fails to localize about 20% of all queries. This is caused by a lack of correct feature matches for these queries, either due to failures of the feature detector or descriptor. DenseSfM skips feature detection and directly matches densely extracted CNN descriptors (which encode higher-level information compared to the gradient histograms used by RootSIFT). This enables DenseSfM to localize more images at a higher accuracy, resulting in the best performance on this dataset. Still, there is significant room for improvement, even in the coarse-precision regime (*cf*. Tab. 3). Also, extracting and matching dense descriptors is a time-consuming task.

5.2. Evaluation on the RobotCar Seasons Dataset

The focus of the RobotCar Seasons dataset is to measure the impact of different seasons and illumination conditions on pose estimation accuracy in an urban environment.

Tab. 4 shows that changing day-time conditions have only a small impact on pose estimation accuracy for all methods. The reason is that seasonal changes have little im-

	Aachen				CMU													
	day			night		foliage			mixed foliage			no foliage			urban			suburban			park		
m	.25/.50/5.0			0.5/1.0/5.0		.25/.50/5.0			.25/.50/5.0			.25/.50/5.0			.25/.50/5.0			.25/.50/5.0			.25/.50/5.0		
deg	2/5/10			2/5/10		2/5/10			2/5/10			2/5/10			2/5/10			2/5/10			2/5/10		
Active Search	57.3	83.7	96.6	19.4	30.6	43.9	28.8	32.5	35.9	25.1	29.4	33.9	52.5	59.4	66.7	55.2	60.3	65.1	20.7	25.9	29.9	12.7	16.3	20.8
CSL	52.3	80.0	94.3	24.5	33.7	49.0	16.3	19.1	26.0	15.2	18.8	28.6	36.5	43.2	57.5	36.7	42.0	53.1	8.6	11.7	21.1	7.0	9.6	17.0
DenseVLAD	0.0	0.1	22.8	0.0	2.0	14.3	13.2	31.6	82.3	16.2	38.1	85.4	17.8	42.1	91.3	22.2	48.7	92.8	9.9	26.6	85.2	10.3	27.0	77.0
NetVLAD	0.0	0.2	18.9	0.0	2.0	12.2	10.4	26.1	80.1	11.0	26.7	78.4	11.8	29.1	82.0	17.4	40.3	93.2	7.7	21.0	80.5	5.6	15.7	65.8
FABMAP	0.0	0.0	4.6	0.0	0.0	0.0	1.1	2.7	16.5	1.0	2.5	14.7	3.6	7.9	30.7	2.7	6.4	27.3	0.5	1.5	13.6	0.8	1.7	11.5
LocalSfM				36.7	54.1	72.4	55.4	57.0	59.9	52.4	55.1	58.6	70.8	72.7	75.9	72.8	74.1	76.1	55.2	57.7	61.3	41.8	44.5	48.7
DenseSfM				39.8	60.2	84.7																		
AS+GC(seq)							86.6	93.0	99.3	76.3	88.5	99.8	77.6	86.8	99.8	86.4	93.6	99.8	92.0	96.0	99.7	71.0	84.0	99.2

Table 3. Evaluation on the **Aachen Day-Night** dataset and a subset of the conditions of the **CMU Seasons** dataset.

	day conditions							night conditions	
	dawn	dusk	OC-summer	OC-winter	rain	snow	sun	night	night-rain
m	.25 / .50 / 5.0	.25 / .50 / 5.0	.25 / .50 / 5.0	.25 / .50 / 5.0	.25 / .50 / 5.0	.25 / .50 / 5.0	.25 / .50 / 5.0	.25 / .50 / 5.0	.25 / .50 / 5.0
deg	2 / 5 / 10	2 / 5 / 10	2 / 5 / 10	2 / 5 / 10	2 / 5 / 10	2 / 5 / 10	2 / 5 / 10	2 / 5 / 10	2 / 5 / 10
ActiveSearch	36.2 / 68.9 / 89.4	44.7 / 74.6 / 95.9	24.8 / 63.9 / 95.5	33.1 / 71.5 / 93.8	51.3 / 79.8 / 96.9	36.6 / 72.2 / 93.7	25.0 / 46.5 / 69.1	0.5 / 1.1 / 3.4	1.4 / 3.0 / 5.2
CSL	47.2 /73.3 / 90.1	56.6 / 82.7 / 95.9	34.1 / 71.1 / 93.5	39.5 / 75.9 / 92.3	59.6 / 83.1 / 97.6	53.2 / 83.6 / 92.4	28.0 / 47.0 / 70.4	0.2 / 0.9 / 5.3	0.9 / 4.3 / 9.1
DenseVLAD	8.7 / 36.9 / 92.5	10.2 / 38.8 / 94.2	6.0 / 29.8 / 92.0	4.1 / 26.9 / 93.3	10.2 / 40.6 / 96.9	8.6 / 30.1 / 90.2	5.7 / 16.3 / 80.2	0.9 / 3.4 / 19.9	1.1 / 5.5 / 25.5
NetVLAD	6.2 / 22.8 / 82.6	7.4 / 29.7 / 92.9	6.5 / 29.6 / 95.2	2.8 / 26.2 / 92.6	9.0 / 35.9 / 96.0	7.0 / 25.2 / 91.8	5.7 / 16.5 / 86.7	0.2 / 1.8 / 15.5	0.5 / 2.7 / 16.4
FABMAP	1.2 / 5.6 / 14.9	4.1 / 18.3 / 55.1	0.9 / 8.9 / 39.3	2.6 / 13.3 / 44.1	8.8 / 32.1 / 86.5	2.0 / 8.2 / 28.4	0.0 / 0.0 / 2.4	0.0 / 0.0 / 0.0	0.0 / 0.0 / 0.0

Table 4. Evaluation on the **RobotCar Seasons** dataset. We report the percentage of queries localized within the three thresholds.

	all day	all night
m	.25 / .50 / 5.0	.25 / .50 / 5.0
deg	2 / 5 / 10	2 / 5 / 10
ActiveSearch	35.6 / 67.9 / 90.4	0.9 / 2.1 / 4.3
CSL	45.3 / 73.5 / 90.1	0.6 / 2.6 / 7.2
ActiveSearch+GC (triplet)	45.5 / 77.0 / 94.7	2.7 / 6.9 / 12.1
ActiveSearch+GC (sequence, GT)	46.7 / 80.1 / 97.0	5.8 / 21.0 / 43.1
seqSLAM	1.3 / 6.1 / 15.3	0.2 / 0.7 / 1.5

Table 5. Using **multiple images** for pose estimation (ActiveSeach+GC) on the **RobotCar Seasons** dataset.

		RobotCar - all night
	m	.25 / .50 / 5.0
	deg	2 / 5 / 10
ActiveSearch	full model	0.9 / 2.1 / 4.3
	sub-model	3.2 / 7.9 / 12.0
CSL	full model	0.6 / 2.6 / 7.2
	sub-model	0.5 / 2.8 / 13.4
ActiveSearch+GC (triplet)	full model	2.7 / 6.9 / 12.1
	sub-model	7.4 / 15.3 / 27.0
ActiveSearch+GC (sequence, GT)	full model	5.8 / 21.0 / 43.1
	sub-model	13.3 / 35.9 / 61.8
ActiveSearch+GC (sequence, VO)	full model	1.5 / 7.4 / 22.9
	sub-model	3.6 / 12.5 / 42.2
LocalSfM	sub-model	16.1 / 27.3 / 44.1

Table 6. Using **location priors** to query only submodels rather than the full **RobotCar Seasons** dataset for night-time queries.

pact on the building facades that are dominant in most query images. The exceptions are "dawn" and "sun". For both, we observed overexposed images caused by direct sunlight (*cf*. Fig. 1). Thus, fewer features can be found for Active Search and CSL and the global image descriptors used by the image retrieval approaches are affected as well.

On the Aachen Day-Night dataset, we observed that image retrieval-based methods (DenseVLAD and NetVLAD) consistently performed worse than structure-based methods (Active Search, CSL, LocalSfM, and DenseSfM). For the RobotCar dataset, NetVLAD and DenseVLAD essentially achieve the same coarse-precision performance as Active Search and CSL. This is caused by the lower variation in viewpoints as the car follows the same road.

Compared to Aachen, there is an even stronger drop in pose accuracy between day and night for the RobotCar dataset. All methods fail to localize a significant number of queries for both the high- and medium-precision regimes. Interestingly, DenseVLAD and NetVLAD outperform all other methods in the coarse-precision regime (*cf*. Fig. 4(right)). This shows that their global descriptors still encode distinctive information even if local feature matching fails. The better performance of all methods under "night+rain" compared to "night" comes from the autoexposure of the RobotCar's cameras. A longer exposure is used for the "night", leading to significant motion blur.

Multi-image queries. The RobotCar is equipped with three synchronized cameras and captures sequences of images for each camera. Rather than querying with only a single image, we can thus also query with multiple photos. Tab. 5 shows the results obtained with seqSLAM (which uses temporal sequences of all images captured by the three cameras) and Active Search+GC. For the latter, we query with triplets of images taken at the same time as well as with temporal sequences of triplets. For the triplets, we use the known extrinsic calibration between the three cameras mounted on the car. For the temporal sequences, we use relative poses obtained from the ground truth (GT) absolute poses. For readability, we only show the results summarized for day- and night-conditions.

Tab. 5 shows that Active Search+GC consistently outperforms single image methods in terms of pose accuracy. Active Search+GC is able to accumulate correct matches over multiple images. This enables Active Search+GC to succeed even if only a few matches are found for each individual image. Naturally, the largest gain can be observed when using multiple images in a sequence.

Location priors. In all previous experiments, we considered the full RobotCar 3D model for localization. However, it is not uncommon in outdoor settings to have a rough

prior on the location at which the query image was taken. We simulate such a prior by only considering the sub-model relevant to a query rather than the full model. While we observe only a small improvement for day-time queries, localizing night-time queries significantly benefits from solving an easier matching problem (*cf*. Tab. 6). For completeness, we also report results for LocalSfM, which also considers only a small part of the model relevant to a query. Active Search+GC outperforms LocalSfM on this easier matching task when querying with sequences. This is due to not relying on one single image to provide enough matches.

One drawback of sequence-based localization is that the relative poses between the images in a sequence need to be known quite accurately. Tab. 6 also reports results obtained when using our own multi-camera visual odometry (VO) system to compute the relative poses. While performing worse compared to ground truth relative poses, this more realistic baseline still outperforms methods using individual images. The reasons for the performance drop are drift and collapsing trajectories due to degenerate configurations.

5.3. Evaluation on the CMU Seasons Dataset

Compared to the urban scenes shown in the other datasets, significant parts of the CMU Seasons dataset show suburban or park regions. Seasonal changes can drastically affect the appearance of such regions. In the following, we thus focus on these conditions (see [53] for an evaluation of all conditions). For each query image, we only consider its relevant sub-model.

Tab. 3 evaluates the impact of changes in foliage and of different regions on pose accuracy. The reference condition for the CMU Seasons dataset does not contain foliage. Thus, other conditions for which foliage is also absent lead to the most accurate poses. Interestingly, DenseVLAD and NetVLAD achieve a better performance than Active Search and CSL for the medium- and coarse-precision regimes under the "Foliage" and "Mixed Foliage" conditions. For the coarse-precision regime, they even outperform LocalSfM. This again shows that global image-level descriptors can capture information lost by local features.

We observe a significant drop in pose accuracy in both suburban and park regions. This is caused by the dominant presence of vegetation, leading to many locally similar (and thus globally confusing) features. LocalSfM still performs well as it only considers a few reference images that are known to be a relevant for a query image. Again, we notice that DenseVLAD and NetVLAD are able to coarsely localize more queries compared to the feature-based methods.

Localizing sequences (Active Search+GC) again drastically helps to improve pose estimation accuracy. Compared to the RobotCar Seasons dataset, where the sequences are rather short (about 20m maximum), the sequences used for the CMU Seasons dataset completely cover their corresponding sub-models. In practical applications, smaller sequences are preferable to avoid problems caused by drift when estimating the relative poses in a sequence. Still, the results from Tab. 3 show the potential of using multiple rather than a single image for camera pose estimation.

6. Conclusion & Lessons Learned

In this paper, we have introduced three challenging new benchmark datasets for visual localization, allowing us, for the first time, to analyze the impact of changing conditions on the accuracy of 6DOF camera pose estimation. Our experiments clearly show that the long-term visual localization problem is far from solved.

The extensive experiments performed in this paper lead to multiple interesting conclusions: (i) Structure-based methods such as Active Search and CSL are robust to most viewing conditions in urban environments. Yet, performance in the high-precision regime still needs to be improved significantly. (ii) Localizing night-time images against a database built from day-time photos is a very challenging problem, even when a location prior is given. (iii) Scenes with a significant amount of vegetation are challenging, even when a location prior is given. (iv) SfM, typically used to obtain ground truth for localization benchmarks, does not fully handle problems (ii) and (iii) due to limitations of existing local features. Dense CNN feature matching inside SfM improves pose estimation performance at high computational costs, but does not fully solve the problem. Novel (dense) features, *e.g.*, based on scene semantics [57], seems to be required to solve these problems. Our datasets readily provide a benchmark for such features through the LocalSfM and DenseSfM pipelines. (v) Image-level descriptors such as DenseVLAD can succeed in scenarios where local feature matching fails. They can even provide coarse-level pose estimates in autonomous driving scenarios. Aiming to improve pose accuracy, *e.g.*, by denser view sampling via synthetic images [67] or image-level approaches for relative pose estimation, is an interesting research direction. (vi) There is a clear benefit in using multiple images for pose estimation. Yet, there is little existing work on multi-image localization. Fully exploiting the availability of multiple images (rather than continuing the focus on single images) is thus another promising avenue for future research.

Acknowledgements. This work was partially supported by ERC grant LEAP No. 336845, CIFAR Learning in Machines & Brains program, EU-H2020 project LADIO 731970, the European Regional Development Fund under the project IMPACT (reg. no. CZ.02.1.01/0.0/0.0/15_003/0000468), JSPS KAKENHI Grant Number 15H05313, EPSRC Programme Grant EP/M019918/1, the Swedish Research Council (grant no. 2016-04445), the Swedish Foundation for Strategic Research (Semantic Mapping and Visual Navigation for Smart Robots), and Vinnova / FFI (Perceptron, grant no. 2017-01942).

References

[1] R. Arandjelović, P. Gronat, A. Torii, T. Pajdla, and J. Sivic. NetVLAD: CNN architecture for weakly supervised place recognition. In *Proc. CVPR*, 2016. 2, 3, 5

[2] R. Arandjelović and A. Zisserman. Three things everyone should know to improve object retrieval. In *Proc. CVPR*, 2012. 3, 6

[3] R. Arandjelović and A. Zisserman. DisLocation: Scalable descriptor distinctiveness for location recognition. In *Proc. ACCV*, 2014. 2

[4] H. Badino, D. Huber, and T. Kanade. Visual topometric localization. In *Proc. IV*, 2011. 2, 5

[5] P. J. Besl and N. D. McKay. Method for registration of 3-D shapes. *IEEE PAMI*, 14(2):239–256, 1992. 5

[6] J.-L. Blanco-Claraco, F.-Á. Moreno-Dueñas, and J. González-Jiménez. The Málaga urban dataset: High-rate stereo and LiDAR in a realistic urban scenario. *IJRR*, 33(2):207–214, 2014. 2

[7] E. Brachmann, A. Krull, S. Nowozin, J. Shotton, F. Michel, S. Gumhold, and C. Rother. DSAC - Differentiable RANSAC for Camera Localization. In *Proc. CVPR*, 2017. 3, 6

[8] E. Brachmann, F. Michel, A. Krull, M. Y. Yang, S. Gumhold, and C. Rother. Uncertainty-driven 6d pose estimation of objects and scenes from a single rgb image. In *Proc. CVPR*, 2016. 3

[9] F. Camposeco, T. Sattler, A. Cohen, A. Geiger, and M. Pollefeys. Toroidal Constraints for Two-Point Localization under High Outlier Ratios. In *Proc. CVPR*, 2017. 2

[10] F. Camposeco, T. Sattler, and M. Pollefeys. Minimal Solvers for Generalized Pose and Scale Estimation from Two Rays and One Point. In *Proc. ECCV*, 2016. 3

[11] S. Cao and N. Snavely. Graph-based discriminative learning for location recognition. In *Proc. CVPR*, 2013. 3

[12] S. Cao and N. Snavely. Minimal Scene Descriptions from Structure from Motion Models. In *Proc. CVPR*, 2014. 1

[13] N. Carlevaris-Bianco, A. K. Ushani, and R. M. Eustice. University of Michigan North Campus long-term vision and lidar dataset. *IJRR*, 35(9):1023–1035, 2016. 2, 3

[14] D. M. Chen, G. Baatz, K. Köser, S. S. Tsai, R. Vedantham, T. Pylvänäinen, K. Roimela, X. Chen, J. Bach, M. Pollefeys, B. Girod, and R. Grzeszczuk. City-Scale Landmark Identification on Mobile Devices. In *Proc. CVPR*, 2011. 2, 3

[15] Z. Chen, A. Jacobson, N. Sünderhauf, B. Upcroft, L. Liu, C. Shen, I. D. Reid, and M. Milford. Deep learning features at scale for visual place recognition. In *Proc. ICRA*, 2017. 2, 3

[16] S. Choudhary and P. J. Narayanan. Visibility probability structure from sfm datasets and applications. In *Proc. ECCV*, 2012. 2

[17] R. Clark, S. Wang, A. Markham, N. Trigoni, and H. Wen. VidLoc: A Deep Spatio-Temporal Model for 6-DoF Video-Clip Relocalization. In *Proc. CVPR*, 2017. 3

[18] M. Cummins and P. Newman. FAB-MAP: Probabilistic Localization and Mapping in the Space of Appearance. *IJRR*, 27(6):647–665, 2008. 2, 3, 5

[19] M. Donoser and D. Schmalstieg. Discriminative Feature-to-Point Matching in Image-Based Locallization. In *Proc. CVPR*, 2014. 2

[20] J. Engel, T. Schöps, and D. Cremers. LSD-SLAM: Large-scale direct monocular SLAM. In *Proc. ECCV*, 2014. 3

[21] M. Fischler and R. Bolles. Random Sampling Consensus: A Paradigm for Model Fitting with Application to Image Analysis and Automated Cartography. *Commun. ACM*, 24:381–395, 1981. 4

[22] D. Gálvez-López and J. D. Tardos. Bags of binary words for fast place recognition in image sequences. *T-RO*, 28(5):1188–1197, 2012. 2

[23] A. Geiger, P. Lenz, C. Stiller, and R. Urtasun. Vision meets robotics: The KITTI dataset. *IJRR*, 32(11):1231–1237, 2013. 2

[24] P. Gronat, J. Sivic, G. Obozinski, and T. Pajdla. Learning and calibrating per-location classifiers for visual place recognition. *IJCV*, 118(3):319–336, 2016. 3

[25] R. Hartley, J. Trumpf, Y. Dai, and H. Li. Rotation Averaging. *IJCV*, 103(3):267–305, 2013. 5

[26] A. Irschara, C. Zach, J.-M. Frahm, and H. Bischof. From Structure-from-Motion Point Clouds to Fast Location Recognition. In *Proc. CVPR*, 2009. 2, 3

[27] H. Jégou, M. Douze, C. Schmid, and P. Pérez. Aggregating local descriptors into a compact image representation. In *Proc. CVPR*, 2010. 2

[28] A. Kendall, M. Grimes, and R. Cipolla. PoseNet: A Convolutional Network for Real-Time 6-DOF Camera Relocalization. In *Proc. ICCV*, 2015. 2, 3, 6

[29] L. Kneip, D. Scaramuzza, and R. Siegwart. A Novel Parametrization of the Perspective-Three-Point Problem for a Direct Computation of Absolute Camera Position and Orientation. In *Proc. CVPR*, 2011. 4

[30] V. Larsson, J. Fredriksson, C. Toft, and F. Kahl. Outlier rejection for absolute pose estimation with known orientation. In *Proc. BMVC*, 2016. 1

[31] G. H. Lee, B. Li, M. Pollefeys, and F. Fraundorfer. Minimal solutions for the multi-camera pose estimation problem. *IJRR*, 34(7):837–848, 2015. 3, 6

[32] Y. Li, N. Snavely, D. Huttenlocher, and P. Fua. Worldwide Pose Estimation Using 3D Point Clouds. In *Proc. ECCV*, 2012. 1, 2, 3

[33] Y. Li, N. Snavely, and D. P. Huttenlocher. Location Recognition using Prioritized Feature Matching. In *Proc. ECCV*, 2010. 1, 2, 3, 4

[34] C. Linegar, W. Churchill, and P. Newman. Work smart, not hard: Recalling relevant experiences for vast-scale but time-constrained localisation. In *Proc. ICRA*, 2015. 3

[35] C. Linegar, W. Churchill, and P. Newman. Made to measure: Bespoke landmarks for 24-hour, all-weather localisation with a camera. In *Proc. ICRA*, 2016. 3

[36] L. Liu, H. Li, and Y. Dai. Efficient Global 2D-3D Matching for Camera Localization in a Large-Scale 3D Map. In *Proc. ICCV*, 2017. 2

[37] D. Lowe. Distinctive Image Features from Scale-Invariant Keypoints. *IJCV*, 60(2):91–110, 2004. 3, 6

[38] S. Lowry, N. Sünderhauf, P. Newman, J. J. Leonard, D. Cox, P. Corke, and M. J. Milford. Visual place recognition: A survey. *IEEE Transactions on Robotics*, 32(1):1–19, 2016. 2

[39] S. Lynen, T. Sattler, M. Bosse, J. Hesch, M. Pollefeys, and R. Siegwart. Get Out of My Lab: Large-scale, Real-Time Visual-Inertial Localization. In *Proc. RSS*, 2015. 1, 2

[40] W. Maddern, M. Milford, and G. Wyeth. CAT-SLAM: probabilistic localisation and mapping using a continuous appearance-based trajectory. *IJRR*, 31(4):429–451, 2012. 3

[41] W. Maddern, G. Pascoe, C. Linegar, and P. Newman. 1 Year, 1000km: The Oxford RobotCar Dataset. *IJRR*, 36(1):3–15, 2017. 2, 4

[42] M. Milford, S. Lowry, N. Sunderhauf, S. Shirazi, E. Pepperell, B. Upcroft, C. Shen, G. Lin, F. Liu, C. Cadena, et al. Sequence searching with deep-learnt depth for condition-and viewpoint-invariant route-based place recognition. In *Proc. CVPR Workshops*, 2015. 3

[43] M. J. Milford and G. F. Wyeth. SeqSLAM: Visual route-based navigation for sunny summer days and stormy winter nights. In *Proc. ICRA*, 2012. 2, 3

[44] P. Mühlfellner, M. Bürki, M. Bosse, W. Derendarz, R. Philippsen, and P. Furgale. Summary maps for lifelong visual localization. *Journal of Field Robotics*, 2015. 3

[45] R. Mur-Artal, J. M. M. Montiel, and J. D. Tards. ORB-SLAM: A Versatile and Accurate Monocular SLAM System. *T-RO*, 31(5):1147–1163, 2015. 2

[46] T. Naseer, G. L. Oliveira, T. Brox, and W. Burgard. Semantics-aware visual localization under challenging perceptual conditions. In *ICRA*, 2017. 2, 3

[47] T. Naseer, L. Spinello, W. Burgard, and C. Stachniss. Robust visual robot localization across seasons using network flows. In *Proc. AAAI*, 2014. 3

[48] R. Pless. Using Many Cameras as One. In *Proc. CVPR*, 2003. 3, 5

[49] F. Radenović, J. L. Schönberger, D. Ji, J.-M. Frahm, O. Chum, and J. Matas. From Dusk till Dawn: Modeling in the Dark. In *Proc. CVPR*, 2016. 2

[50] T. Sattler, M. Havlena, F. Radenovic, K. Schindler, and M. Pollefeys. Hyperpoints and fine vocabularies for large-scale location recognition. In *Proc. ICCV*, 2015. 1, 2

[51] T. Sattler, M. Havlena, K. Schindler, and M. Pollefeys. Large-scale location recognition and the geometric burstiness problem. In *Proc. CVPR*, 2016. 2

[52] T. Sattler, B. Leibe, and L. Kobbelt. Efficient & Effective Prioritized Matching for Large-Scale Image-Based Localization. *IEEE PAMI*, 39(9):1744–1756, 2017. 1, 2

[53] T. Sattler, W. Maddern, C. Toft, A. Torii, L. Hammarstrand, E. Stenborg, D. Safari, M. Okutomi, M. Pollefeys, J. Sivic, F. Kahl, and T. Pajdla. Benchmarking 6DOF Outdoor Visual Localization in Changing Conditions. *arXiv:1707.09092*, 2018. 6, 8

[54] T. Sattler, A. Torii, J. Sivic, M. Pollefeys, H. Taira, M. Okutomi, and T. Pajdla. Are Large-Scale 3D Models Really Necessary for Accurate Visual Localization? In *Proc. CVPR*, 2017. 1, 2, 3, 5

[55] T. Sattler, T. Weyand, B. Leibe, and L. Kobbelt. Image Retrieval for Image-Based Localization Revisited. In *Proc. BMVC*, 2012. 2, 3

[56] J. L. Schönberger and J.-M. Frahm. Structure-From-Motion Revisited. In *Proc. CVPR*, June 2016. 3

[57] J. L. Schönberger, M. Pollefeys, A. Geiger, and T. Sattler. Semantic Visual Localization. In *Proc. CVPR*, 2018. 3, 8

[58] J. Shotton, B. Glocker, C. Zach, S. Izadi, A. Criminisi, and A. Fitzgibbon. Scene Coordinate Regression Forests for Camera Relocalization in RGB-D Images. In *Proc. CVPR*, 2013. 2, 3

[59] K. Simonyan and A. Zisserman. Very deep convolutional networks for large-scale image recognition. In *Proc. ICLR*, 2015. 6

[60] J. Sivic and A. Zisserman. Video Google: A text retrieval approach to object matching in videos. In *Proc. ICCV*, 2003. 3

[61] X. Sun, Y. Xie, P. Luo, and L. Wang. A Dataset for Benchmarking Image-Based Localization. In *Proc. CVPR*, 2017. 2, 3

[62] N. Sünderhauf, F. Dayoub, S. Shirazi, B. Upcroft, and M. Milford. On the Performance of ConvNet Features for Place Recognition. In *Proc. IROS*, 2015. 3

[63] N. Sünderhauf, P. Neubert, and P. Protzel. Are we there yet? Challenging SeqSLAM on a 3000 km journey across all four seasons. In *Proc. ICRA Workshops*, 2013. 2, 3, 5

[64] N. Sünderhauf, S. Shirazi, A. Jacobson, F. Dayoub, E. Pepperell, B. Upcroft, and M. Milford. Place Recognition with ConvNet Landmarks: Viewpoint-Robust, Condition-Robust, Training-Free. In *Proc. RSS*, 2015. 2, 3

[65] L. Svärm, O. Enqvist, F. Kahl, and M. Oskarsson. City-Scale Localization for Cameras with Known Vertical Direction. *IEEE PAMI*, 39(7):1455–1461, 2017. 1, 2, 5

[66] H. Taira, M. Okutomi, T. Sattler, M. Cimpoi, M. Pollefeys, J. Sivic, T. Pajdla, and A. Torii. InLoc: Indoor Visual Localization with Dense Matching and View Synthesis. In *Proc. CVPR*, 2018. 1

[67] A. Torii, R. Arandjelović, J. Sivic, M. Okutomi, and T. Pajdla. 24/7 Place Recognition by View Synthesis. In *Proc. CVPR*, 2015. 2, 3, 5, 8

[68] A. Torii, J. Sivic, M. Okutomi, and T. Pajdla. Visual Place Recognition with Repetitive Structures. *IEEE PAMI*, 2015. 3

[69] A. Torii, J. Sivic, M. Okutomi, and T. Pajdla. Visual place recognition with repetitive structures. *IEEE PAMI*, 2015. 2

[70] F. Walch, C. Hazirbas, L. Leal-Taixé, T. Sattler, S. Hilsenbeck, and D. Cremers. Image-Based Localization Using LSTMs for Structured Feature Correlation. In *Proc. ICCV*, 2017. 3

[71] S. Wang, M. Bai, G. Mattyus, H. Chu, W. Luo, B. Yang, J. Liang, J. Cheverie, S. Fidler, and R. Urtasun. TorontoCity: Seeing the World With a Million Eyes. In *Proc. ICCV*, 2017. 2

[72] T. Weyand, I. Kostrikov, and J. Philbin. Planet - photo geolocation with convolutional neural networks. In *Proc. ECCV*, 2016. 3

[73] B. Zeisl, T. Sattler, and M. Pollefeys. Camera pose voting for large-scale image-based localization. In *Proc. ICCV*, 2015. 1, 2